Earth and Planetary Science
https://journals.nasspublishing.com/index.php/eps

ARTICLE

Storm-Time Variability of GNSS-Derived Ionospheric VTEC over East Africa during Four Major Geomagnetic Storms of Solar Cycle 24

Wilberforce Muniafu [1*] **, *Edward Uluma*** [1,2] **, *Solomon Otoo Lomotey*** [3] **, *Atirsaw Muluye Tilahun*** [4] **, *Moses Mefe*** [5] **, *Joseph Kagotho Muriithi*** [6,7] **, *George Omondi*** [8] **, *Boniface Ndinya*** [1]

[1] *Department of Physics, Masinde Muliro University of Science & Technology, Kakamega 50100, Kenya*

[2] *Department of Science Technology and Engineering, Kibabii University, Bungoma 50200, Kenya*

[3] *Department of Physical and Mathematical Sciences, University of Environment and Sustainable Development, PMB, Somanya, Ghana*

[4] *Department of Physics, College of Natural and Computational Science, Wachemo University, Hosaena 667, Ethiopia*

[5] *Department of Geomatics, Ahmadu Bello University, Zaria 810221, Nigeria*

[6] *Department of Space Science and Astronomy, Kenya Space Agency, Nairobi 00100, Kenya*

[7] *Department of Physics, University of Nairobi, Nairobi 00200, Kenya*

[8] *Department of Physics and Materials Science, Maseno University, Maseno 40105, Kenya*

ABSTRACT

This study investigates the ionospheric response to four major geomagnetic storms during solar cycle 24 (18–19 February, 2014, Dst minimum −119 nT; 17–18 March, 2015, Dst minimum −223 nT; 22–23 June, 2015, Dst minimum −204 nT; and 8 September, 2017, Dst minimum −142 nT) using Vertical Total Electron Content (VTEC) data derived from Global Navigation Satellite System (GNSS) observations over the East African region. Our results revealed substantial storm-time VTEC variability characterized by both positive and negative ionospheric phases. The main phases of the storms had significant VTEC enhancements, especially near the Equatorial Ionization Anomaly

*CORRESPONDING AUTHOR:
Wilberforce Muniafu, Department of Physics, Masinde Muliro University of Science & Technology, Kakamega 50100, Kenya;
Email: muniafuw@gmail.com

ARTICLE INFO
Received: 17 January 2026 | Revised: 23 March 2026 | Accepted: 25 March 2026 | Published Online: 10 April 2026
DOI: https://doi.org/10.36956/eps.v5i1.3205

CITATION
Muniafu, W., Uluma, E., Lomotey, S.O., et al., 2026. Storm-Time Variability of GNSS-Derived Ionospheric VTEC over East Africa during Four Major Geomagnetic Storms of Solar Cycle 24. Earth and Planetary Science. 5(1): 75–92. DOI: https://doi.org/10.36956/eps.v5i1.3205

(EIA) crest. This was attributed to the intensified equatorial fountain process which was primarily driven by Prompt Penetration Electric Fields (PPEF). In contrast, reductions in VTEC were observed during quiet periods. This was attributed to the effect of Disturbance Dynamo Electric Fields (DDEF), compositional changes in the upper atmosphere and storm-induced thermospheric winds. Clear spatial differences in VTEC responses across the GNSS stations were noted, indicating a strong influence of the equatorial electrodynamics on ionospheric variability. The results underscore the critical role of GNSS observations in monitoring space weather impacts and enhancing the understanding of storm-time ionospheric dynamics over the equatorial East African region, which has historically remained underexplored.

Keywords: Geomagnetic Storm; Total Electron Content; Equatorial Ionization Anomaly; Disturbance Dynamo Electric Field; Equatorial Ionosphere

1. Introduction

The ionosphere is the ionized part of the upper atmosphere from about 50 km to 1,000 km above sea level. It is formed through ionization of neutral atmospheric constituents by solar extreme ultra-violet (EUV) radiation and X-ray radiation. Due to increased free electrons in this region, any disturbance can affect the propagation of the radio signals used in satellite communication, radar applications and navigation systems by changing their speed and direction of propagation [1]. The increased accumulation of free electrons in the ionosphere affects the electromagnetic waves passing through it by inducing an additional transmission time delay [2]. The time delay is directly proportional to the abundance number of free electrons in a cylinder of unit cross section along the signal path extending from the satellite to the receiver on the ground and inversely proportional to the square of the frequency of the trans-ionospheric radio wave, which is referred to as Total Electron Content (TEC) [3–5]. The ionospheric dynamics in the equatorial region are quite unique and complex, due to the unique geometry of the magnetic field and low inclination in the region. The plasma density structure in the ionosphere shows significant variations with time of day, latitude, longitude, season, solar and geomagnetic activity. These variations affect TEC, which in turn significantly affects radio wave propagation [1] through fading and phase scintillation of L-band navigation signals like the ones used by Global Navigation Satellite Systems (GNSS) [6]. Geomagnetic storms are among the primary drivers of ionospheric disturbances. These storms are often triggered by eruptions from the Sun's corona, which release large amounts of plasma and magnetic fields into space in the form of coronal mass ejections (CMEs). When directed towards Earth, CMEs interact with the geomagnetic field, generating intense geomagnetic storms that can disrupt radio communications and affect power systems on the ground. Geomagnetic storms are disturbances of the Earth's magnetic field as a result of perturbations in the Interplanetary Magnetic Field [7]. There are two effects of geomagnetic storms on ionospheric density: they can either lead to an enhancement in plasma density (positive effect) or decrease in plasma density (negative effect) [8]. The increase in electron density is attributed to the intensification of the equatorial fountain, and this is caused by Prompt Penetration Electric Field (PPEF)-induced eastward electric field enhancement. The effect of storm-time equatorward neutral winds, which slow down both downward diffusion of plasma and the recombination process, may also lead to a positive effect [9]. The decrease in O/N_2 ratio at low latitudes, which is caused by a change in neutral composition at low latitudes, leads to a negative Ionospheric effect [10].

Several studies have examined the ionospheric response to geomagnetic storms in different regions of the world. For instance, Feng et al. [11] investigated the ionospheric responses to the 17 March, 2017 and 22 June, 2015 geomagnetic storms over the Wuhan region using GNSS-based tomographic technique and reported negative storm effects during the geomagnetic storm, which were attributed to the effects such as DDEF and PPEF, changes in neutral composition from

the high latitudes. Similarly, Habyarimana et al.[12] investigated ionospheric storm time effects over the East African sector during the 17 March, 2013, and 2015 geomagnetic storms in the solar cycle 24. The study aimed to identify similarities and differences between the two storms since they occurred during the same period and season. Their results showed that the ionospheric responses to the two storms over the equatorial and low-latitude region of East Africa were as a result of the combined effects of the equatorward neutral wind and PPEF and DDEF. Other studies within Africa also reported strong VTEC variability associated with geomagnetic disturbance[13,14]. In the East African region, several investigations have also been conducted to examine ionospheric TEC using GNSS observations. Uluma et al.[15] analyzed the variability of TEC gradient and TEC rate index over Kisumu, Kenya, during selected quiet and storm days of 2013 and 2014 using RINEX data archived in the SCIntillation Network Decision Aid (SCINDA) situated at Maseno, Kenya. The study showed that Ionospheric irregularities developed mostly after sunset hours during both geomagnetically quiet days, with more intense irregularities being observed during geomagnetically disturbed days. Aol et al.[16] studied the effects of space weather on the ionosphere during an intense geomagnetic storm of 17–28 February 2014 over Mbarara (MBAR). The location of the East Africa region within the Equatorial Ionization anomaly (EIA) region makes it sensitive to storm-time disturbances. Muniafu et al.[17] further studied the ionospheric VTEC response to the intense geomagnetic storm of 10–11 May, 2024 using 6 GNSS stations spread over low, mid, and high latitudes. The study revealed that the equatorial stations, MBAR and BELE displayed an increase in Vertical TEC (VTEC), which was attributed to the intensified effects of PPEF. Muniafu et al.[18] investigated the ionospheric response of the 17 March and 22 June, 2015 geomagnetic over East African stations. The study revealed that the storm impacts varied with local time and season, with greater effects being observed during the equinox period. Despite the increasing number of studies on ionospheric disturbances, the East African sector remains relatively underexplored compared to South American and Southeast Asian equatorial regions due to scarcity of data. Furthermore, the existing studies in East Africa have majorly focused on single storm events or isolated stations which limit the understanding of broad spatial structure and storm-time ionospheric dynamics. This study addresses that gap by examining ionospheric responses during multiple geomagnetic storm events within solar cycle 24: the 17–18 February, 2014 (Dst = ~123 nT); the St. Patricks' Day storm of 17–18 March, 2015 (Dst = ~229 nT); and the June solstice storm of 22–23 June, 2015 (Dst = ~204 nT) and 8 September, 2017 (Dst = ~144 nT). The purpose of this study is to provide a clear understanding of spatial and temporal dynamics of equatorial ionosphere in the East African sector during four major geomagnetic storms of solar cycle 24. Unlike the previous works, which focused only on the March 2015 and June 2015 geomagnetic storms, the present manuscript provides a comprehensive multi-storm investigation of four major geomagnetic storms during Solar Cycle 24. The manuscript further incorporates comparative seasonal analysis, solar cycle phase dependence, detailed latitudinal electrodynamic variability, thermospheric O/N_2 composition effects, and the coupling between PPEF, DDEF, and Traveling Ionospheric Disturbances (TIDs) over the East African equatorial region

2. Data Acquisition and Methodology

2.1. Data Sources

2.1.1. Geomagnetic Indices Data

In this study, the z-component of interplanetary magnetic field (IMF-Bz), y-component of interplanetary electric field (IEF-Ey), solar wind speed (SWS), planetary K-index (Kp) and Disturbance storm time (Dst) indices were obtained from Omniweb website (accessed online): https://omniweb.gsfc.nasa.gov/form/dx1.html. **Table 1** gives a summary of major geomagnetic storms in solar cycle 24, their classification and their minimum Dst values.

Table 1. Summary of four major geomagnetic storms in solar cycle 24.

Storm	Date	Minimum Dst (nT)	Classification
Feb 2014	18–19 Feb, 2014	−120	Intense
Mar 2015	17–18 Mar, 2015	−223	Intense
Jun 2015	22–23 Jun, 2015	−200	Intense
Sep 2017	8 Sept, 2017	−142	Intense

In this study, the criteria for categorizing geomagnetic storms were adopted as follows: weak storms (Dst > −50 nT), moderate storms (−100 nT < Dst < −50 nT), and intense storms (Dst ≤ −100 nT) [19].

2.1.2. GNSS Data

GNSS-TEC data were obtained from seven (7) GNSS receiver stations whose geographic and geomagnetic locations are shown in **Table 2**. The selection of stations was guided by the need to ensure adequate spatial coverage across latitudes within the East African equatorial region. ADIS and MBAR, located close to the geomagnetic equator, are particularly sensitive to equatorial ionospheric processes. MAL2 and MBEY extend both the latitudinal and longitudinal coverage, enabling comparative analysis across different latitudinal zones. In addition, MOIU, DODM, and ARSH enhance longitudinal representation, improving the ability to monitor spatial variations and track ionospheric disturbances across the East African region.

Table 2. Geographic and geomagnetic coordinates of the GNSS stations.

GNSS Station	Geographic Latitude	Geographic Longitude	Geomagnetic Latitude	Geomagnetic Longitude	Local Time (LT) Conversion
ADIS	9.04° N	38.77° E	0.18° N	110.49° E	LT = UT + 3
ARSH	3.38° S	36.69° E	12.83° S	108.6° E	LT = UT + 3
DODM	6.19° S	35.75° E	16.10° S	107.22° E	LT = UT + 3
MOIU	0.29° N	35.29° E	4.27° S	106.94° E	LT = UT + 3
MAL2	2.99° S	40.19° E	7.28° S	111.47° E	LT = UT + 3
MBAR	0.61° S	30.65° E	10.22° S	102.36° E	LT = UT + 3
MBEY	9.03° S	33.43° E	18.89° S	104.56° E	LT = UT + 3

Geographical coordinates were converted to geomagnetic coordinates using the World Data Center for Geomagnetism website accessed through the link https://www.ukssdc.ac.uk/cgi-bin/wdcc1/coordcnv.pl.

The geographical positions of the 7 GNSS receiver stations are given in **Figure 1**. The GNSS-TEC data for the storm days and the five quiet days with Dst 0 nT to 20 nT obtained from the World Data Center for Geomagnetism, Kyoto, via the website: https://wdc.kugi.kyoto-u.ac.jp/ for each storm event were accessed from the University of NAVSTAR Consortium website: https://gage-data.earthscope.org/archive/gnss/rinex/obs.

2.1.3. Thermospheric Composition

The global maps showing the ratio of O/N_2 for the period 17–19 February, 2014, 16–18 March, 2015, 21–23 June, 2015 and 7–9 September, 2017 were obtained from the GUVI mission datasets which are available online (using the website: https://guvitimed.jhuapl.edu/guvi-galleryl3on2).

The O/N_2 ratio was used as a proxy for thermospheric energy input and composition change. In this regard, increases in O/N_2 ratio indicate enhanced ionization, resulting from positive ionospheric storm phase while decreases in O/N_2 ratio indicates enhanced recombination, resulting from negative ionospheric storm phase.

2.2. Methodology

2.2.1. TEC Processing

These GNSS-TEC data were processed into VTEC using the GNSS-TEC processing software developed by Seemala and Valladares [20]. The TEC analysis software (version 3.5) uses the phase and code values for both L1 and L2 frequencies to eliminate the effect of clock errors and tropospheric water vapor to calculate relative values of slant TEC (STEC) [21–23] as

$$STEC = \frac{1}{40.3}\left[\frac{{f_1}^2 {f_2}^2}{{f_1}^2 - {f_2}^2}\right](p_2 - p_1) \quad (1)$$

where f_1 and f_2 are the GNSS carrier frequencies, and p_1 and p_2 represent pseudo-range measurements at the respective frequencies.

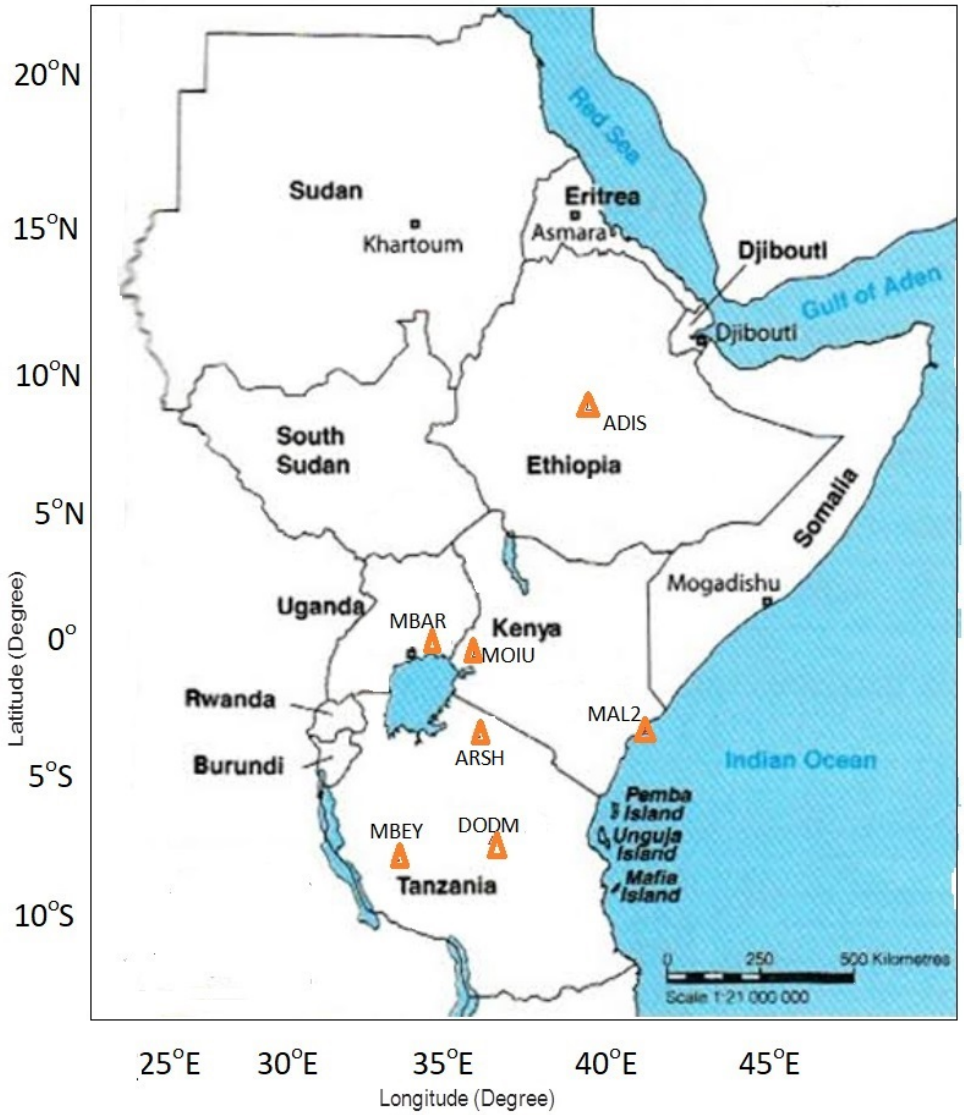

Figure 1. The Geographic locations of ADIS, ARSH, MOIU, MAL2, MBAR, DODM and MBEY.

The STEC values can be converted to VTEC using thin shell approximation at the Ionospheric pierce point (IPP)

$$VTEC = STEC \times cos\,(\chi), \quad (2)$$

where is the zenith angle (χ) is given by

$$\chi = arcsin\left[\frac{R_E \cos\theta}{R_E + h}\right], \quad (3)$$

where θ is the elevation angle of the satellite at the IPP in degrees, R_E is the Earth's radius is equal to 6,378.137 km and h is the Height of the Ionospheric layer, assuming a thin-shell ionospheric height of 350 km [24]. The ionospheric height over the low latitude region is highly variable (shows both seasonal and diurnal dependence) and is also influenced by fountain effect. In the low latitude region, it ranges between 350 and 600 km [25,26]. A minimum satellite elevation angle cutoff of 40° was applied to reduce multipath effects and measurement errors [27]. Instrumental biases, including satellite and receiver differential code biases (DCBs), were corrected us-

ing standard calibration procedures. The TEC data were smoothed using a moving average filter to reduce short-term fluctuations and measurement noise.

2.2.2. Percentage Change in VTEC

The positive and negative enhancements of VTEC were also computed using the percentage of deviation of VTEC obtained by using Equation (4) [28],

$$\%\Delta TEC = \left(\frac{TEC_s - TEC_q}{TEC_q} \right) \times 100 \qquad (4)$$

where, TEC_s is the average VTEC during geomagnetic storm days, TEC_q is the average VTEC during quiet days. Positive 50% indicate enhanced ionization compared to quiet time, while negative 50% indicate VTEC depletion compared to quiet conditions. Quiet days were selected based on low geomagnetic activity (Kp ≤ 2 and Dst > −20 nT) and were used as baseline references.

3. Results

3.1. Variations of Solar Wind and Geomagnetic Parameters

Figure 2a–d shows the temporal variation of the z-component of interplanetary magnetic field (IMF-Bz), solar wind speed (SWS), y-component of interplanetary electric field (IEF-Ey) and disturbance storm time (Dst) for 17–19 February, 2014; 21–23 June, 2015; 16–18 March, 2015 and 7–9 September, 2017 respectively. In **Figure 2a**, the IMF-Bz turned southward (−15 nT) on 19 February, 2014 at 06:00–11:00 UT, signifying energy transfer into the magnetosphere. A corresponding enhancement of IEF-Ey to 5 mV/m was observed, showing the presence of strong convection electric fields. The solar wind speed (SWS) increased moderately to 600–700 km/s, an indication of coronal mass ejection (CME) driven storm. The Dst index dropped to −120 nT, depicting the commencement of moderate to strong geomagnetic storm. In **Figure 2b**, the IMF-Bz sharply turned southward (−25 nT) on 22 June, 2015 at 12:00–23:00 UT, with a corresponding enhancement of IEF-Ey of up to 18 mV/m. The SWS increased to 700 km/s, which was an indication of a fast-moving CME. The southward turning of the Dst reached its minimum −200 nT, an indication of a severe geomagnetic storm. In **Figure 2c**, the IMF-Bz sharply turned southward (−21 nT) on 17 March, 2015 at 06:00–20:00 UT, with a corresponding enhanced IEF-Ey of up to 10 mV/m. The SWS increased up to 600–700 km/s, showing a fast CME. The Dst index value dropped to its minimum of −250 nT, depicting one of the most intense storms of Solar Cycle 24. In **Figure 2d**, the IMF-Bz sharply turned southward (−21 nT) on 8 September, 2017 at 00:00, with a corresponding enhanced IEF-Ey of up to 18 mV/m. The SWS increased up to 800 km/s, an indication of a fast CME. The Dst index value dropped to its minimum of −150 nT, an indication of a strong storm.

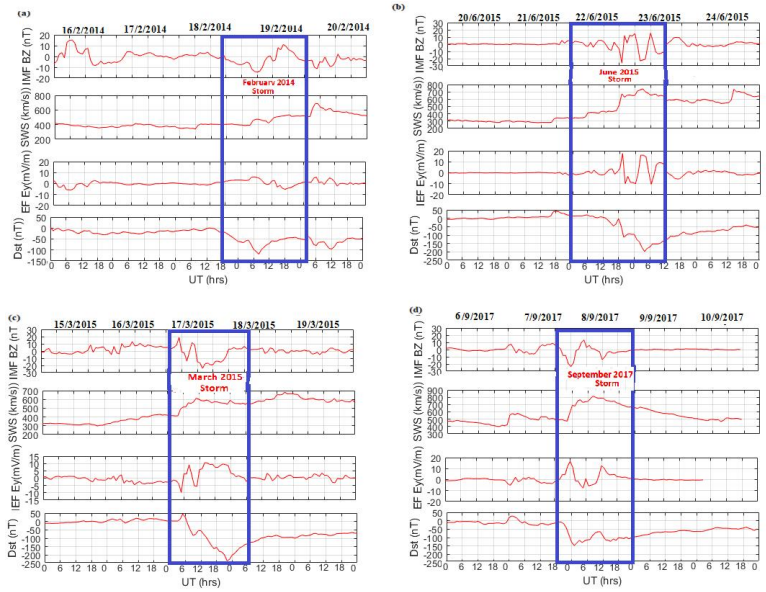

Figure 2. Variations of IMF Bz, solar wind speed, IEF-Ey and Dst index for (**a**) 16–20 February 2014, (**b**) 20–24 June 2015, (**c**) 15–19 March 2015, (**d**) 6–10 September 2017.

3.2. Global O/N_2 Map Ratio

Figure 3a–d presents the global distribution of thermospheric O/N_2 ratio during the study periods: 17–19 February, 2014; 16–18 March, 2015; 21–23 June, 2015 and 7–9 September, 2017, respectively. The spatial variations give insights into storm-time changes in thermospheric composition, which directly influences ionospheric electron density via ion production and recombination processes.

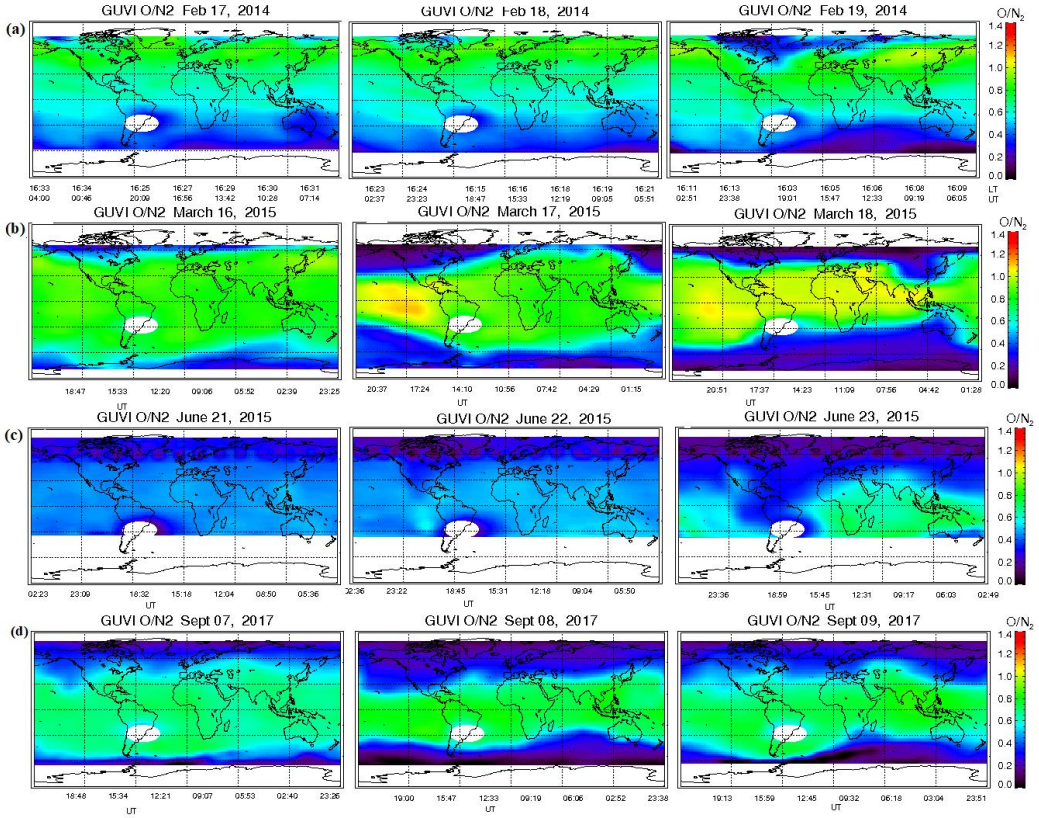

Figure 3. Global O/N_2 map ratio for: (**a**) 17–19 February, 2014, (**b**) 16–18 March, 2015, (**c**) 21–23 June, 2015, (**d**) 7–9 September, 2017.

Note: accessed from GUVI mission datasets accessed on18th October 2025.

Generally, the Global O/N_2 ratio maps in **Figure 3** show that storm-time thermospheric composition changes are global but tend to vary latitudinally and longitudinally depending on geomagnetic conditions, storm intensity and the local time.

In **Figure 3a**, on 17–19 February, 2014 the O/N_2 ratio was moderate (0.6–0.8) at low and mid latitude regions. These observed results suggest an increase in atomic oxygen relative to molecular nitrogen, hence higher ion production rates. In **Figure 3b**, on 16–18 March, 2015 there was a decrease in O/N_2 ratio in high latitude with values below 0.2 on both hemispheres while the equatorial and mid-latitude the ratio was 0.9 indicating an increase in oxygen atom when compared to nitrogen atoms. In **Figure 3c**, on 21–23 June, 2015 there was reduced O/N_2 ratio globally (below 0.4), an indication of a relaxed thermosphere following the main phase of the storm. In **Figure 3d**, on 7–9, September 2017 the O/N_2 ratio displayed intense enhancements at the equatorial and mid-latitude regions, an indication of large–scale thermospheric composition changes.

3.3. Variation of VTEC

Figure 4 shows temporal variations of VTEC over ADIS, DODM, MBAR, ARSH, MAL2, MOIU and MBEY for 16–20 February, 2014; 15–19 March, 2015; 20–24 June, 2015 and 6–10 September, 2017.

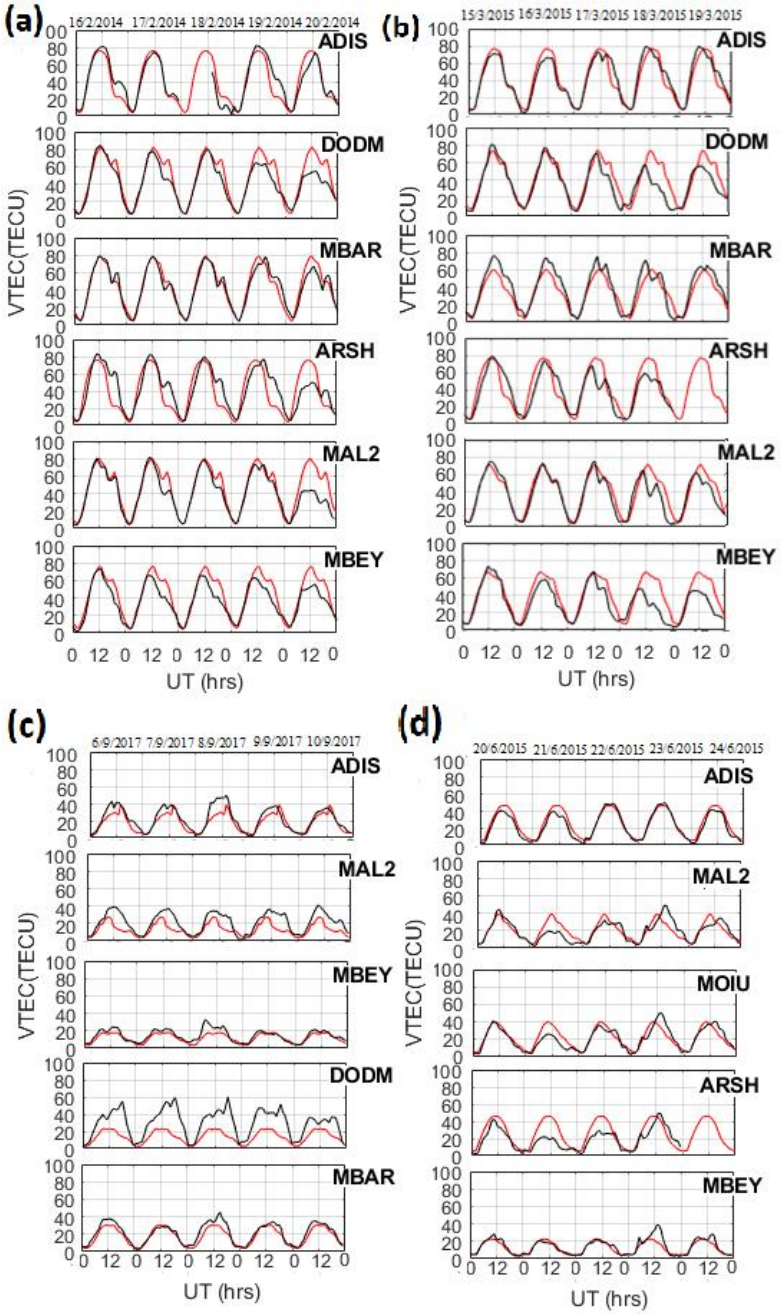

Figure 4. VTEC variations over: (**a**) ADIS, DODM, MBAR, ARSH, MAL2, MBEY for 16–20 February, 2014, (**b**) ADIS, DODM, MBAR, ARSH, MAL 2, MBEY for 15–19 March, 2015, (**c**) ADIS, MAL2, MBEY, DODM, MBAR for 6–10 September, 2017, (**d**) ADIS, MAL2, MOIU, ARSH, MBEY for 20–24 June, 2015.

In **Figure 4a,b**, the VTEC profiles exhibited typical diurnal patterns characterized by low VTEC values at 00:00–06:00 UT (nighttime), gradual VTEC increase at 06:00–08:00 UT (sunrise), pronounced VTEC peaks at 10:00–14:00 UT (local noon) and a decline in VTEC after 14:00 UT towards evening period. This observed pattern is a reflection of the normal ionospheric response to solar radiation, where photoionization leads to an increase in electron density during the day while recombination of ions and electrons in the absence of solar radiation at night leads to reduction in electron density. The diurnal variation of VTEC was in total agreement with that reported by Fayose et al.[29] on VTEC variation and their effect on GNSS over Akure in Nigeria in 2010. MBAR and ARSH showed moderate daytime VTEC peaks of 78–80 TECU. DODM and ADIS showed larger daytime

VTEC peaks of 80–82 TECU as compared to MBEY and MAL2 which had lower daytime VTEC peaks of 60–80 TECU for both 16–20 February, 2014 and 15–19 March, 2015. These observed differences were attributed to the effect of the Equatorial Ionization Anomaly (EIA) and local electrodynamic variations [30]. ADIS and DODM are situated at the EIA crest and hence experience stronger ionization. Dual VTEC peaks were observed over most stations and were attributed to the post-sunset effects or the EIA crest movement. In **Figure 4c**, the daytime VTEC peaks for most stations from 6–10 September, 2017 ranged between 20–60 TECU while in **Figure 4d**, the daytime VTEC peaks for most stations from 20–24 June, 2015 ranged between 20–50 TECU. In **Figure 4c**, MAL2, MBEY and DODM showed noticeable VTEC deviations and irregular patterns, depicting disturbed ionospheric conditions. However, MBAR and ADIS exhibited relatively regular diurnal VTEC variations. The weaker daytime TEC peaks across all the stations from 6–10 September, 2017 might be attributed to seasonal effects associated with the September equinox transition period. In **Figure 4d**, ADIS recorded the highest VTEC peak of 50 TECU; this was attributed to its proximity to the EIA. MOIU and MAL2 showed moderate VTEC peaks while MBEY and ARSH displayed lower VTEC peaks. These peak TEC variations across the stations highlighted the latitudinal dependence.

Comparing **Figure 4c,d** (September, 2017 and June, 2015 geomagnetic storms) and **Figure 4a,b** (February, 2014 and March, 2015 geomagnetic storms), the VTEC values tended to reduce with the decline in the phase of solar cycle 24. This was attributed to the reduction in background ionization levels of VTEC. Despite the GNSS stations displaying lower VTEC values during the September 2017 and June 2015 geomagnetic storms, i.e., **Figure 4c,d**, several stations exhibited irregular VTEC structures and short-lived deviations. These features indicated the presence of storm-driven electrodynamic processes and travelling ionospheric disturbances (TIDs). All the GNSS stations showed spatial variability, which was an indication of non-uniform distribution of ionospheric disturbances across the region, which were strongly influenced by latitude and local time electrodynamic conditions.

3.4. Variation of Percentage Change in VTEC

Figure 5a–d quantifies storm-time ionospheric variability by presenting the percentage VTEC deviation relative to quiet-time conditions over ADIS, MAL2, MBEY, DODM, MBAR, ARSH and MOIU.

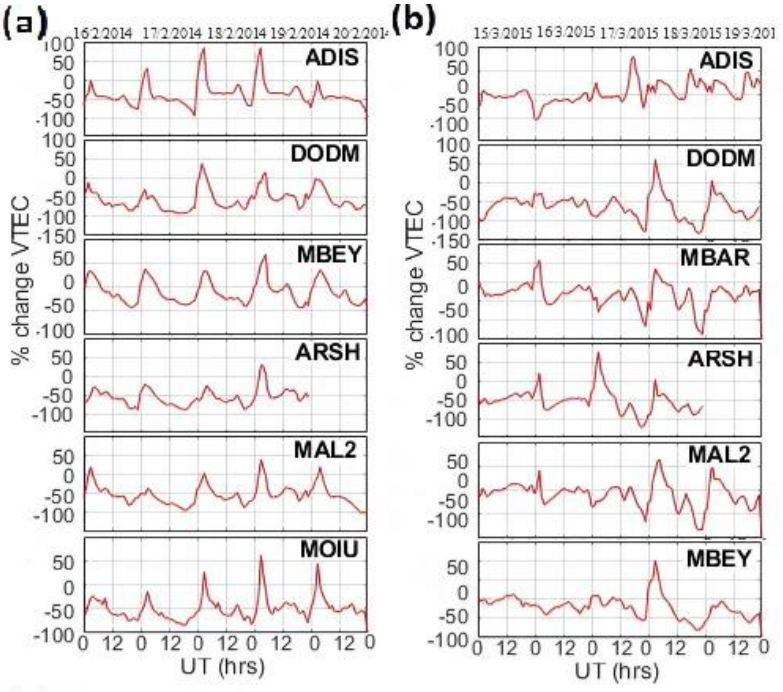

Figure 5. *Cont.*

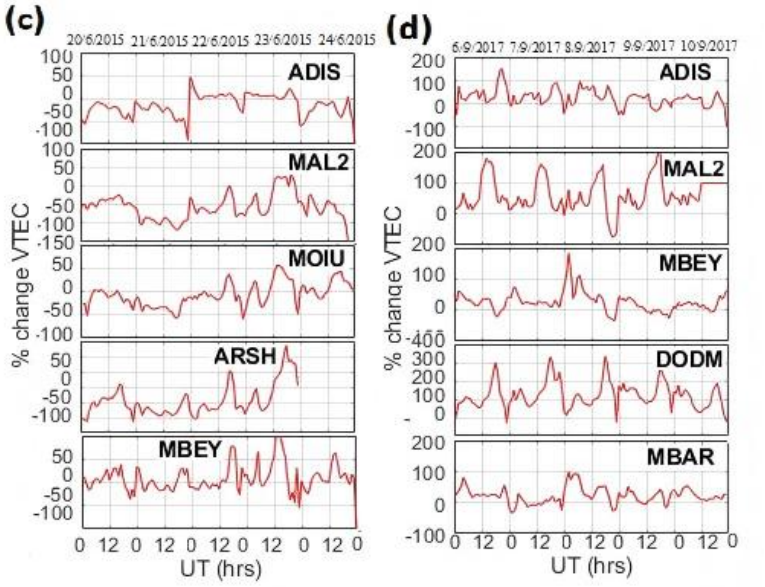

Figure 5. % change in VTEC over: (**a**) ADIS, DODM, MBEY, ARSH, MAL2, MOIU for 16–20 February 2014, (**b**) ADIS, DODM, MBAR, ARSH, MAL2, MBEY for 15–19 March 2015, (**c**) ADIS, MAL2, MOIU, ARSH, MBEY for 16–20 September 2017, (**d**) ADIS, MAL2, MBEY, DODM, MBAR for 6–10 September 2017.

In **Figure 5a,b**, percentage VTEC deviations were revealed across different days during the February, 2014 and March, 2015 geomagnetic storms, highlighting the dynamic nature of the ionospheric electron density in response to varying solar and geomagnetic conditions. In **Figure 5c**, smaller and smoother variations of percentage VTEC were observed across all the stations. The percentage deviation of VTEC ranged within ±50% range, with peaks approaching 80–100%. DODM, MOIU and ADIS displayed moderate percentage VTEC enhancements at local noon, which corresponded with normal diurnal VTEC increase resulting from solar ionization. MAL2, ARSH and MBEY, however showed relatively low percentage VTEC deviation. The observed troughs and crests corresponded majorly to solar-driven diurnal variations. In **Figure 5b**, stronger and irregular deviations were observed, especially from 16–18 March, 2015 (St. Patrick's Day Geomagnetic storm). DODM and ADIS recorded sharp positive enhancements exceeding +50%, which were followed by stronger negative phases (depletions) of 80–140%. MBEY, MAL2, ARSH and MBAR also displayed irregular variations with magnitudes ranging between +50% and −130%. The percentage VTEC deviations observed in **Figure 5a,b** were associated with storm-induced electrodynamic disturbances, which included DDEFs which caused delayed depletion, PPEFs which caused rapid ionization enhancements and also possible thermospheric winds surges and TIDs which affected VTEC gradients.

In **Figure 5a,b**, ADIS and DODM experienced largest percentage VTEC changes which were consistent with strong equatorial electrodynamics and EIA effects. ARSH, MBEY and MAL2 which are situated at higher latitudes showed lower percentage VTEC amplitudes. This was attributed to the damping of the storm effects with respect to their positions from the EIA crest.

Generally, during the February 2014 geomagnetic storm **Figure 5a**, the percentage VTEC deviations remained within moderate ranges of +20% and −20%, which was an indication of small perturbations in ionospheric electron density. In contrast, the March, 2015 geomagnetic storm (**Figure 5b**), the percentage VTEC showed significantly larger deviations ranging between +50% and −140%. The large VTEC percentage deviations were an indication of intense storm-time electrodynamic forcing.

In **Figure 5c**, the percentage VTEC deviation displayed moderate and smoother variations as compared to the percentage VTEC plots in **Figure 5d**, which showed larger, highly fluctuating and more irregular variations. In **Figure 5c**, the percentage VTEC deviations over ADIS, MAL2, MOIU, ARSH and MBEY ranged within ±100%. Weak percentage TEC enhancements of up to

+60% were observed over ARSH and MOIU. ADIS, MAL2, MOIU and ARSH displayed smooth and smaller percentage VTEC variations. MBEY experienced more percentage VTEC deviation, which was attributed to the localized ionospheric wave activity or minor TIDs.

In **Figure 5d**, the percentage VTEC plots over ADIS, MAL2, MBEY, DODM and MBAR showed larger amplitudes ranging between ±150–±300%. These large percentage VTEC deviations signified presence of strong ionospheric disturbances associated with geomagnetic activity. Irregular peaks and troughs signified the influence of short-time electrodynamics such as PPEFs, DDEFs and TIDs. DODM and ADIS and ASH showed more pronounced percentage TEC deviations, which were consistent with their proximity to EIA and magnetic equator—a region sensitive to electrodynamic forcing. MBAR, MAL2 and MBEY displayed VTEC deviations but with a low percentage, an indication that the ionospheric disturbances extended to lower latitudes.

Figure 6 summarizes maximum VTEC values for 16–20 February, 2014; 15–19 March, 2015, 20–24 June, 2015 and 6–10 September, 2017 over ADIS, DODM, MBAR, ARSH, MAL2, MBEY and MOIU. In the figure, larger maximum VTEC values were observed across all stations on 16–20 February, 2014 and 15–19 March, 2015. However, 20–24 June, 2015 and 6–10 September, 2017 exhibited smaller maximum VTEC values. This indicated that maximum VTEC values reduced with the decline of the solar activity. This was attributed to the reduction in background ionization levels.

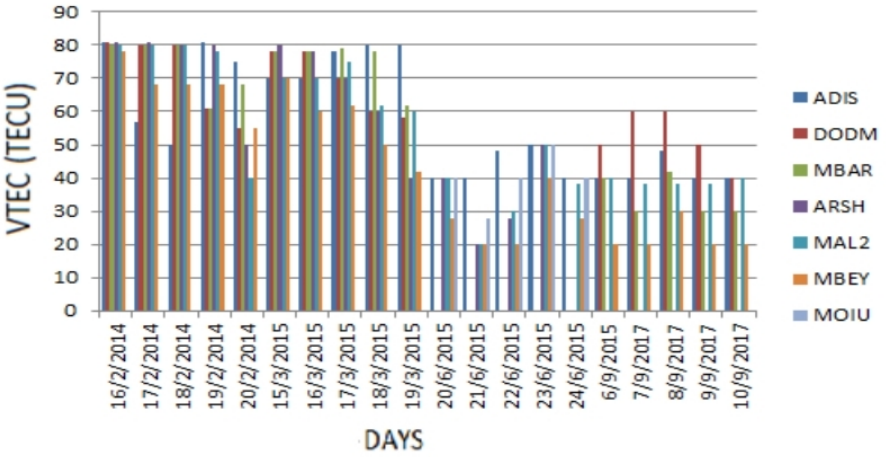

Figure 6. Maximum VTEC for 16–20 February 2014, 15–19 March 2015, 20–24 June 2015 and 6–10 September 2017 over ADIS, DODM, MBAR, ARSH, MAL2, MBEY and MOIU.

4. Discussion

In the study, the analysis of solar wind parameters and geomagnetic indices in **Figure 2** gave a strong indication that the four storms were triggered by the southward turning of the IMF-Bz, which was accompanied by enhanced solar wind speed and IEF-Ey. Studies have shown that prolonged southward turning of the IMF-Bz allows for efficient energy transfer from the solar wind into the magnetosphere through magnetic reconnection, which leads to a reduction in the Dst index [30]. The magnetospheric disturbances were then propagated to the East African low latitude ionosphere. The GNSS-TEC observations in **Figure 4a–d** revealed diurnal typical patterns which were characterized by low values during nighttime, followed by gradual increases after sunrise, peak values at midday (local noon) and gradual decreases towards sunset. This observed behavior was attributed to the effect of solar radiation where photoionization dominated during the day, while recombination processes reduced electron density during nighttime [29]. Storm-time periods displayed VTEC profiles having irregular deviations and enhanced variability as compared to the quiet periods. The irregular deviations and enhanced variability of VTEC indicated presence of storm-time induced electrodynamic processes and TIDs, which modified the distribution of background ionospheric plasma instabilities [31–34].

Positive and negative ionospheric storm phases were observed across the GNSS stations in **Figure 5a–d**. The observed rapid VTEC enhancements during the main phases of the geomagnetic storms, particularly over stations located near the Equatorial Ionization Anomaly (EIA) crest, together with the strong southward turning of IMF-Bz and enhanced IEF-Ey, strongly suggest the penetration of eastward PPEFs into the East African equatorial ionosphere. The occurrence of the VTEC enhancements during daytime and post-sunrise local time hours further supports the role of local time–dependent electrodynamic processes, since eastward PPEFs are known to intensify the upward E × B plasma drift more effectively during daytime conditions, thereby enhancing the equatorial fountain effect and increasing VTEC over the EIA crest regions. The positive ionospheric enhancements were attributed to the effects of PPEFs, which rapidly penetrated the magnetosphere into low-latitude ionosphere during onset of a geomagnetic storm [10]. The eastward directed PPEF intensified the equatorial fountain by lifting ionospheric plasma upwards at the geomagnetic equator and diffusing it to higher latitudes along magnetic field lines. This led to enhanced ionization near the EIA crests, hence increased VTEC values [35]. The global O/N_2 ratio maps in **Figure 3** clearly displayed significant spatial variations in thermospheric composition during geomagnetic storm periods [6,36]. The increased O/N_2 ratios at mid and low-latitudes indicated increased concentrations of atomic oxygen relative to molecular nitrogen, which favored production of ions, leading to enhanced ionospheric electron densities. In contrast, reduced O/N_2 ratios corresponded to increased molecular species that enhanced recombination processes, which led to depletion of plasma. This was a clear indication that the short-time ionospheric variability was also influenced by electrodynamic forcing and thermospheric neutral composition. Negative ionospheric storm effects were also observed across the GNSS receiver stations during certain phases, i.e., **Figure 5a–d**. These negative phases were characterized by VTEC depletions and large negative percentage VTEC deviations relative to quiet-time conditions [9]. The VTEC reductions were attributed to several mechanisms including DDEFs [37,38] and storm-induced thermospheric circulation. During the geomagnetic storm periods, joule heating and particle precipitation at high latitudes generated PPEFs, which produced westward electric fields during the day and suppressed the equatorial fountain [39]. This led to reduced plasma uplift which lowered VTEC values after the main phase of some geomagnetic storms.

A clear latitudinal dependence of storm-time ionospheric variability was also displayed across the GNSS receiver stations. GNSS stations located closer to the geomagnetic equator and EIA crest (DODM and ADIS) exhibited stronger VTEC enhancements and larger percentage of VTEC deviations as compared to GNSS stations that were situated farther away (MBEY, MAL2 and ARSH), i.e., **Figures 4a–d** and **5a–d**. The observed spatial variability, with higher VTEC values at stations near the Equatorial Ionization Anomaly (EIA) crest, revealed the important role played by the equatorial electrodynamics in modulating ionospheric response to geomagnetic storms. The PPEF-driven enhancement of the equatorial fountain effect led to redistribution of plasma from the magnetic equator to low latitudes, intensifying ionization at the anomaly crests [40]. The latitudinal gradients observed in this study were consistent with the expected behavior of the EIA during disturbed geomagnetic conditions. The influence of solar cycle phase on VTEC variability was also observed. The storms occurring during solar maximum of solar cycle 24 exhibited higher maximum VTEC values compared to storms occurring during the declining phase of the solar cycle. This was attributed to the declining solar activity during the declining phase of solar cycle 24. These results were consistent with previous studies, showing the effect of solar cycle phases on ionospheric ionization levels and storm-time responses of VTEC [5,41–44].

The behavior of VTEC over MAL2, ADIS, MBAR, DODM, MOIU ARSH and MBEY was strongly controlled by local time. The diurnal variation of VTEC with time over these stations showed characteristics typical to low latitude ionosphere where VTEC was low during predawn, then increased gradually reaching maximum in the afternoon and then gradually decreased after sunset [29,45]. Between 03:00–09:00 UT (06:00–12:00 LT), there was a steady rise of VTEC in all stations. Maxi-

mum TEC was attained at 09:00–12:00 UT (12:00–15:00 LT). This was attributed to solar extreme Ultra Violet (SEUV) radiation which ionized the ionosphere leading to increase in VTEC (photoionization). Huang et al.[10] attributed these enhancements of VTEC at local noon to strong neutral winds blowing equatorward from the high latitude region that pushed plasma away from the earth and its neutral atmosphere along the magnetic field lines. This led to a reduction in recombination of O^+, which interacts with a neutral molecule for efficient recombination, thereby increasing the plasma density. He also attributed VTEC reductions to changes in the composition of the neutral atmosphere at ionosphere heights due to heating and upwelling of the lower atmosphere with its molecular-rich composition, resulting in a decrease in the O/N_2 ratio and enhancing of the recombination of the O^+ plasma. Between 15:00–19:00 UT (18:00–22:00 LT), most stations displayed VTEC depletions which were closely followed by TEC enhancements, with February 2014 geomagnetic storm exhibiting the largest TEC depletions. This was attributed to the pre-reversal enhancement (PRE) and the upward E × B drift. Olwendo et al.[42] observed that the PRE in VTEC effect was an outcome of the interaction of the E and F region dynamos which resulted into an enhancement of the eastward electric field before it turns westward at dusk. The PRE increases the vertical drift which makes the ionosphere to be lifted to higher altitude where the ratio of production to loss of electrons is greater and the transport of ions is dominant. Between 19:00–02:00 UT (22:00–05:00 LT), VTEC values decreased due to domination of recombination, resulting from absence of solar radiation.

The shape of VTEC peaks during geomagnetic storms in **Figures 4** and **5** gave a reflection of the competition between storm-time electrodynamics (DDEF and PPEF) and changes in ionospheric composition (O/N_2 ratio). The February 2014, March 2015, June 2015 and September 2017 geomagnetic storms exhibited both single peak and double peak behavior over all the 7 GNSS receiver stations. Single VTEC peaks across the GNSS stations were exhibited during the February 2014 (**Figure 4a**). This signified presence of weak electric fields which limited uplift of plasma. Double VTEC peaks were exhibited by most GNSS stations during the March 2015 geomagnetic storms (**Figure 4b**). This was indication of presence of strong E × B drift due to PPEFs. During the June 2015 and September 2017 geomagnetic storms, the GNSS stations displayed double VTEC peaks (**Figure 4c**) which were attributed to the interaction of plasma uplift (due to the presence of PPEFs) and the westward directed DDEF[46]. Studies describing various VTEC curve shapes in the Equatorial Ionization Anomaly (EIA) region of Africa have been conducted and shown that the shapes of the peak VTEC curves are recorded at the presence (or absence) of strength of electric currents at the equator in reference to the daily variation of electric currents over time[47]. Studies by Ouattara and Amory-Mazaudier[48] on diurnal behavior of NmF2 at Ouagadougou (Burkina Faso) near the geomagnetic equator and by Pham Thi et al.[49] at Phu Thuy (Vietnam) at the northern crest of the equatorial fountain in Vietnam have shown that VTEC curves with two maximum peaks are dominant near the magnetic equator while the VTEC curves with single peaks are dominant at the crest. Geomagnetic activity modifies the diurnal behavior of the ionosphere manifested through variation in VTEC or NmF2.

The significant VTEC enhancements observed during the main phases of all analyzed storms were attributed to PPEFs. These eastward electric fields originated from enhanced magnetospheric convection and rapidly penetrated to equatorial latitudes. The resulting increase in the upward E × B drift elevated plasma to higher altitudes (where recombination rates are reduced) and led to enhanced electron density. This mechanism explains the pronounced daytime VTEC increases observed during the main phases, particularly during the March, 2015 and June, 2015 geomagnetic storms, where peak values exceeded 90 TECU. The stronger response during these events was consistent with their larger geomagnetic intensity, as indicated by more negative Dst values in **Figure 2**.

The VTEC depletion observed during the recovery phases of the storms was associated with DDEFs. These westward electric fields which are generated by thermospheric wind circulation driven by Joule heating and particle precipitation at high latitudes dur-

ing the disturbance drives meridional winds which in turn travel down to the equatorial region, generating DDEF. Blanc and Richmond [39] reported that DDEF takes about 4–5 h to reach the low-latitude depending on their speed [50] while their ensuing effects are known to last longer during the recovery phase of geomagnetic storms [51]. Unlike PPEFs, gradual and longer persistence of DDEF, leads to suppression of the equatorial fountain effect [40,52,53]. The resulting downward plasma drift enhances recombination rates, contributing to the observed VTEC depletion during the recovery phase as shown in **Figure 4a–d**. The magnitude of VTEC reduction, particularly during the June 2015 storm where values decreased to 30–40 TECU, highlighted the strong influence of disturbance dynamo processes on low-latitude ionospheric dynamics. At low latitudes, during the main phase of a geomagnetic storm (symbolized by the southward turning of IMF-Bz), PPEF may occur and may affect the vertical plasma drift over the region. In the evening or post-evening period, PPEF assumes eastward (or westward) configuration leading to the strengthening (or weakening) of the vertical plasma drift [13,40]. During the recovery phase, DDEF (which has opposite configuration to PPEF) occurs in the evening hours, hence suppressing the pre-reversal enhancement (PRE) drift.

Variations in the thermospheric O/N_2 ratio play a significant role in modulating ionospheric electron density during geomagnetic storms. Increased O/N_2 ratios (shown in **Figure 3**) during the main phase enhanced ion production, contributing to the observed VTEC enhancements in **Figure 4a–d**. Conversely, reduced O/N_2 ratios during the recovery phase promoted recombination, leading to electron density depletion [54,55]. A significant enhancement in the O/N_2 ratio was observed in the lower latitudes and equatorial regions. It was mainly controlled by the thermospheric neutral winds which are related to the Joule heating in high latitudes. The correspondence between reduced O/N_2 ratios and VTEC depletion observed in this study supported the role of thermospheric composition changes in driving negative ionospheric storm effects. These findings highlight the coupled nature of ionospheric and thermospheric processes during geomagnetic disturbances and are in agreement with a study by Li et al. [35].

The observed storm-time ionospheric responses in this study were consistent with findings from studies done in other equatorial regions [12–15,17–19,35], where similar VTEC enhancement and depletion patterns were reported. However, the magnitude and spatial distribution of VTEC variations observed in this study indicated regional differences that may be attributed to longitudinal variations in geomagnetic field configuration and thermospheric dynamics. The multi-station analysis presented here provided a more comprehensive characterization of the East African sector compared to previous studies that relied on single storm, limited spatial coverage or single-station observations.

The results demonstrated that geomagnetic storms produce significant and spatially variable ionospheric disturbances over East Africa. These variations have important implications for GNSS-based navigation and communication systems, which are sensitive to ionospheric delays. The strong VTEC enhancements during storm main phases may introduce significant positioning errors, while recovery phase depletions can affect signal reliability. The findings underscore the importance of continuous GNSS monitoring and regional ionospheric modeling for improved space weather forecasting in this sector.

In summary, the result obtained from this study indicates that storm-time ionospheric variability was largely controlled by equatorial dynamics and thermospheric processes. Furthermore, the study provides insights into spatial characteristics of storm-time ionospheric responses over the GNSS stations in East Africa.

5. Conclusions

This study investigated the ionospheric response to four major geomagnetic storms during solar cycle 24 over East Africa using GNSS-derived VTEC. The analysis revealed pronounced storm-time ionospheric variability characterized by both positive and negative phases. Significant VTEC enhancements were observed during the main phases of the storms, with peak values exceeding 90 TECU at stations near the EIA crest. These enhancements were associated with PPEFs, which intensify the

equatorial fountain and increase plasma density at low latitudes.

In contrast, the recovery phases were characterized by substantial VTEC depletion, with values decreasing to 30–40 TECU in some cases. This behavior is attributed to DDEFs, which suppressed upward plasma drift and enhanced recombination processes. Variations in the thermospheric O/N_2 ratio further modulated ionospheric electron density, reinforcing both positive and negative storm effects. The competition between storm-time electrodynamics (DDEF and PPEF) and changes in ionospheric composition (O/N_2 ratio) was also revealed by the shape of VTEC peaks during geomagnetic storms.

The results also demonstrated clear spatial variability in ionospheric response across East Africa, with stronger effects observed near the EIA crest. This highlights the dominant role of equatorial electrodynamics in controlling regional ionospheric dynamics.

Overall, this study provides a comprehensive multi-event, multi-station characterization of storm-time ionospheric variability over the East African sector, a region that has remained relatively underexplored. The findings contribute to improved understanding of ionosphere–thermosphere coupling processes and have important implications for GNSS-based navigation and space weather monitoring in equatorial regions.

Author Contributions

Conceptualization, W.M., E.U., G.O., and B.N.; methodology, W.M., E.U., G.O., B.N., S.O.L., M.M., J.K.M., and A.M.T.; software, W.M., E.U., S.O.L., M.M., and J.K.M.; validation, W.M., E.U., S.O.L., A.M.T., M.M., J.K.M., and B.N.; formal analysis, W.M., E.U., G.O., B.N., S.O.L., M.M., J.K.M., and A.M.T.; investigation, W.M., E.U., S.O.L., and M.M.; resources, W.M., E.U., and S.O.L.; data curation, W.M., E.U., S.O.L., A.M.T., M.M., and J.K.M.; writing—original, W.M., E.U., S.O.L., and B.N.; draft preparation, W.M., E.U., S.O.L., and A.M.T.; writing—review and editing, W.M., E.U., G.O., B.N., S.O.L., M.M., J.K.M., and A.M.T.; visualization, W.M., E.U., S.O.L., and A.M.T.; supervision, W.M., E.U., G.O., and B.N.; project administration, G.O. and B.N. All authors have read and agreed to the published version of the manuscript.

Funding

This work did not receive any funding.

Institutional Review Board Statement

Not applicable.

Informed Consent Statement

Not applicable.

Data Availability Statement

Data is available and can be obtained from the corresponding author on request.

Acknowledgments

The authors acknowledge the Earthscope Consortium: https://www.earthscope.org for the GNSS data, Omniweb for the solar wind parameters: https://omniweb.gsfc.nasa.gov, GUVI mission: https://guvitimed.jhuapl.edu/guvi-galleryl3on2 for the global O/N_2 maps and Prof Gopi Seemala for the GPS-TEC analysis software. Masinde Muliro University is acknowledged for providing office space, library and internet facilities during the research period.

Conflicts of Interest

The authors declare no conflict of interest.

AI Use Statement

The authors declare that no artificial intelligence (AI) tools were used in the preparation of this manuscript.

References

[1] Ngwira, C., Seemela, G., Habarulema, J., 2013. Simultaneous observations of ionospheric irregularities in the African low-latitude region. Journal of Atmospheric and Solar-Terrestrial Physics. 97, 50–57.

[2] Klobuchar, J.A., Parkinson, B.W., Spillker, J.J., 1996. Ionospheric effect on GPS. In Global Positioning System: Theory and Application. American Institute of Aeronautics and Astronautics: Washington, DC, USA.

[3] Wellenhof, B.H., Lichtenegger, H., Collins, J., 1992. Global Positioning Systems: Theory and Practice. Springer-Verlag Wien: New York, NY, USA.

[4] Misra, P., Enge, P., 2001. Global Positioning System Signals, Measurement and Performance. Ganga Jamuna Press: Lincoln, MA, USA.

[5] Adewale, A.O., Oyeyemi, E.O., Adeloye, A.B., et al., 2012. A Study of L-Band scintillations and total electron content at an Equitorial station Lagos Nigeria. Radio Science. 47(2).

[6] Rodrigues, F.S., Moraes, A.O., de Paula, E.R., et al., 2023. Equatorial plasma bubbles and GNSS scintillation during geomagnetic storms in Solar Cycle 25. Journal of Geophysical Research: Space Physics. 128(11), e2023JA031455.

[7] Pokharia, M., Prasad, I., Bhoj, C., et al., 2018. A study of geomagnetic storms an solar and Interplanetary parameters for solar cycles 22 and 24. Solar Physics. 293(8), 126.

[8] Liu, G., Shen, H., 2017. A severe negative response of ionosphere to the intense geomagnetic storm of 17 March 2015 observed at middle and low latitude stations in China zone. Advances in Space Research. 59(9), 2301–2312. DOI: https://doi.org/10.1016/j.asr.2017.02.021

[9] Lissa, D., Srinivasu, V.K., Prasad, D.S., et al., 2020. Ionospheric response to the 26 August 2018 geomagnetic storm using GPS-TEC observations along 80° E and 120° E longitudes in the Asian sector. Advances in Space Research. 66(6), 1427–1440.

[10] Huang, C., Foster, J.C., Goncherenko, L.P., et al., 2005. A strong postive phase of ionosphere storms observed by the Millstone Hill incoherent Scatter radar and global GPS network. Journal of Geophysical Research. 110(A6).

[11] Feng, J., Zhou, Y., Zhou, Y., et al., 2021. Ionospheric response to the 17 March and 22 June 2015 geomagnetic storms over Wuhan Region using GNSS-based tomographic technigue. Advances in Space Research. 67(1), 111–121.

[12] Habyarimana, V., Habarulema, J., Dugassa, T., 2023. Analysis of ionospheric storm-time effects over the East African sector during the 17 March 2013 and 2015 geomagnetic storms. Earth, Planets and Space. 75(1), 58.

[13] Jonah, O.F., Amory-Mazaudier, C., Doumbia, V., 2023. Equatorial ionospheric irregularities over Africa during geomagnetic disturbance. Advances in Space Research. 72(5), 2010–2025.

[14] Kassa, T., Damtie, B., 2017. Ionospheric irregularities over bahir dar, Ethiopia during selected geomagnetic storms. Advances in Space Research. 60(1), 121–129.

[15] Uluma, E., Ndinya, B., Omondi, G., 2019. Variability of TEC Gradient and TEC Rate Index over Kisumu, Kenya during Selected Quiet and Storm Days of 2013 and 2014. American Journal of Astronomy and Astrophysics. 7(4), 67–72.

[16] Aol, S., Mungufeni, P., Jurua, E., 2019. Effects of space weather on the ionosphere: A case study of geomagnetic storms during 17–28 February 2014. Indian Journal of Radio and Space Physics. 48, 26–37.

[17] Muniafu, W., Uluma, E., Lemotey, S.O., et al., 2024. Ionospheric Total Electron Content Response to the Intense Geomagnetic Storm of 10th–11th May 2024 over Low, Mid and High Latitude Regions. Asian Journal of Research and Reviews in Physics. 8(4), 19–36.

[18] Muniafu, W., Ndinya, B., Omondi, G., 2025. Ionospheric Response to Intense Geomagnetic Storms of 17 March 2015 and 22 June 2015 over the East African region. Journal of Advances in Science Engineering and Technology. 2(1), 26–35.

[19] Gonzalez, W.D., Joselyn, J.A., Kaminde, Y., et al., 1994. What is a geomagnetic storm ?. Journal of Geophysical Research. 99(A4), 5771–5792.

[20] Seemala, G.K., Valladares, C.E., 2011. Statistics of TEC depletions observed over the South American continent for the year 2008. Radio Science. 46(5), RS5019.

[21] Sardon, E., Zarraoa, N., 1997. Estimation of total electron content using GPS data: How stable are differential satellite and receiver instrumental biases?. Radio Science. 32(5), 1899–1910.

[22] Sardon, E., Rius, A., Zarrao, N., 1994. Estimation of the transmitter and receiver differential biases and the ionospheric total electron content from Global positioning system observations. Radio Science. 29(3), 577–586.

[23] Arikan, F., Nayir, H., Sezen, U., et al., 2008. Estimation of single interfrequency receiver bias using GPS-TEC. Radio Science. 43(4), RS4006.

[24] Klobuchar, J.A., 1987. Ionospheric Time-Delay Algorithm for Single-Frequency GPS. IEEE Transactions on Aerospace and Electronic Systems. AES-23(3), 325–331.

[25] Uluma, E., Lomotey, S.O., Bankole, F.J., et al., 2025. Investigation of ionospheric irregularities during the severe geomagnetic storm of 10–11 May 2024. Indian Journal of Physics. 100, 1–19. DOI: https://doi.org/10.1007/s12648-025-03734-6

[26] Opio, P., Andima, G.G., Jurua, E., 2023. Characterization of the effective height of the ionosphere using GPS data over East Africa, a low latitude region. Ad-

vances in Space Research. 71(12), 5196–5207.

[27] Rama Rao, P.V., Niranjan, K., Prasad, D.S., et al., 2006. On the validity of the ionospheric pierce point (IPP) altitude of 350 km in the Indian equatorial and low-latitude sector. Annales Geophysicae. 24(8), 2159–2168.

[28] Tilahun, A.M., Uluma, E., Ejigu, Y.G., 2025. Variation in Total Electron Content During a Severe Geomagnetic Storm, 23–24 April 2023. Atmosphere. 16(6), 676. DOI: https://doi.org/10.3390/atmos16060676

[29] Fayose, R.S., Oladosu, O.R., Rabiu, A.B., et al., 2012. Variation of Total Electron Content [TEC] and their Effect on GNSS over Akure, Nigeria. Applied Physics Research. 4(2), 105–109. DOI: https://doi.org/10.5539/apr.v4n2p105

[30] Belehaki, A., Kutiev, I., Marinov, P., et al., 2017. Ionospheric electron density perturbations during the 7–10 March 2012 geomagnetic storm period. Advances in Space Research. 59(4), 1041–1056.

[31] Oinats, A.W., Nishitani, N., Berngardt, O.I., et al., 2016. Statistical Characteristics of medium-scale travelling ionospheric disturbances revealed from Hokkaido East and Ekaterinburg HF radar data. Earth, Planets and Space. 68, 1–12.

[32] Kelley, M.C., 2011. On origin of mesoscale TIDs at midlatitudes. Annales Geophysicae. 29, 361–366.

[33] Kotake, N., Otsuka, Y., Ogawa, T., et al., 2007. Statistical study of medium-scale Travelling ionospheric distrurbances observed with GPS networks in Southern California. Earth, Planets and Space. 59, 95–102.

[34] Shiokawa, K., Otsuka, Y., Ogawa, T., 2003. Ground-based observations of nighttime medium-scale travelling ionospheric disturbances at middle and low latitudes. Journal of Geophysical Research: Space Physics. 108(A4), 1152.

[35] Li, J., Wang, Y., Yang, S., et al., 2022. Characteristics of low-latitude ionosphere activity and detorioratonof TEC Model during the 7–9 september 2017 magnetic storm. Atmosphere. 13(9), 1365.

[36] Astafyeva, E., Zakharenkova, I., Alken, P., 2016. Prompt penetration electric fields and the extreme topside ionospheric response to the June 22–23, 2015 geomagnetic storm as seen by the swarm constellation. Earth, Planets and Space. 68, 1–12.

[37] Ramsingh, S., Sripathi, S., Sreekumar, S., et al., 2015. Low-latitude ionosphere response to super geomagnetic storm of 17/18 March 2015: Results from a chain of ground-based observations over Indian sector. Journal of Geophysical Research: Space Physics. 120(12), 10864–10882.

[38] Richmond, A., Lu, G., 2000. Upper-atmospheric effects of magnetic storms: a brief tutorial. Journal of Atmospheric and Solar-Terrestrial Physics. 62(12), 1115–1127.

[39] Blanc, M., Richmond, A.D., 1980. The ionospheric disturbance dynamo. Journal of Geophysical Research. 85(A4), 1669–1686. DOI: https://doi.org/10.1029/ja085ia04p01669

[40] Huang, C.S., 2023. Identification of penetration and disturbance dynamo electric fields and their effects on the generation of equatorial plasma bubbles. Journal of Geophysical Research: Space Physics. 128(11), e2023JA031766.

[41] Veenadhari, B., Alex, S., Kikuchi, T., et al., 2010. Penetration of magnetospheric electric fields to the equator and their effects on the low-latitude ionosphere during intense geomagnetic storms. Journal of Geophysical Research. 115(A3). DOI: https://doi.org/10.1029/2009JA014562

[42] Olwendo, J.O., Cilliers, P.J., Baki, P., et al., 2012. Using GPS-SCINDA observations to study the correlation between scintillation, total electron content enhancement and depletions over the Kenyan region. Advances in Space Research. 49(9), 1363–1372.

[43] Dinede, A.H., Kassa, T., 2025. Characterization of equatorial plasma bubbles over the East African sector using the ROTI and Stec depletion. Advances in Space Research. 75(1), 8248–8261.

[44] D'ujanga, F.M., Taabu, S.D., 2014. Study on the occurrence characteristics of VHF and L-band ionospheric Scintillations over East Africa. Indian Journal of Radio and Space Physics. 43, 263–273.

[45] Bagiya, S.M., Joshi, H.P., Iyer, K.N., et al., 2009. TEC variations during low solar activity period (2005-2007) near the Equatorial Ionospheric Anomaly Crest Region in India. Annales Geophysicae. 27, 1047–1057.

[46] Sharma, S., Galav, P., Dashora, N., et al., 2011. Response of low-latitude ionospheric total electron content to the geomagnetic storm of 24 August 2005. Journal of Geophysical Research. 116(A5).

[47] Vassal, J., 1982. Electrojet, counter-electrojet and region F in Sarh (Chad). Géophysique. 19, 3–9. (in French)

[48] Ouattara, F., Amory-Mazaudier, C., 2012. Statistical study of the equatorial F2 layer critical frequency at Ouagadougou during solar cycles 20, 21 and 22, using Legrand and Simon's classification of geomagnetic activity. Journal of Space Weather and Space Climate. 2, A19.

[49] Pham Thi Thu, H., Amory-Mazaudier, C., Huy, M.L., 2011. Time variations of the ionosphere at the northern tropical crest of ionization at Phu Thuy, Vietnam. Annales Geophysicae. 29(1), 197–207.

[50] Poudel, P., Lu, X., 2026. Ionosphere-thermosphere responses to the March 2023 geomagnetic storm using observations and TIEGCM simulations

driven by data assimilated aurora and electric fields. Journal of Geophysical Research: Space Physics. 131(6), e2025JA034954.

[51] Wu, Q., Wang, W., Lin, D., et al., 2024. Penetrating electric field during the Nov 3-4, 2021 geomgnetic storm. Journal of Atmospheric and Solar-Terrestrial Physics. 257, 106219.

[52] Fejer, B.G., Laranja, N.G., Condor, P., 2024. Multiprocess driven unusually large equatorial perturbation electric fields during the April 2023 geomagnetic storm. Frontiers in Astronomy and Space Sciences. 11, 1351735.

[53] Abdu, M.A., Nogueira, P.A.B., Santos, A.M., et al., 2018. Impact of disturbance electric fields in the evening on prereversal vertical drift and spread F developments in the equatorial ionosphere. Annales Geophysicae. 36, 609–620.

[54] Kirchman, J.A., Hysell, D.A., Nicolls, M.J., 2025. Persistence of the prereversal enhancement of the equatorial vertical plasma drifts observed by ICON. Geophysical Research Letters. 52.

[55] Stephan, A.W., Meier, R.R., England, S.L., et al., 2025. Ionospheric and thermospheric response to the 13 June 2022 M-class solar flare. Journal of Geophysical Research: Space Physics. 130(5), e2024JA0333526.